Hindawi
Wireless Power Transfer
Volume 2023, Article ID 9998972, 14 pages
https://doi.org/10.1155/2023/9998972



*Research Article*

# Optimizing Energy Storage System Operations and Configuration through a Whale Optimization Algorithm Enhanced with Chaotic Mapping and IoT Data: Enhancing Efficiency and Longevity of Energy Storage Stations

**Meizhen Gao**

*Jiaozuo Normal College, Henan, Jiaozuo 454000, China*

Correspondence should be addressed to Meizhen Gao; gmz1970@jzsz.edu.cn

Received 22 May 2023; Revised 23 October 2023; Accepted 1 November 2023; Published 4 December 2023

Academic Editor: Chan Hwang See



To enhance the charging and discharging strategy of the energy storage system (ESS) and optimize its economic efficiency, this paper proposes a novel approach based on the enhanced whale algorithm. Recognizing that the standard whale algorithm can sometimes suffer from local optima in high-dimensional multiobjective optimization, this study introduces chaotic mapping and individual information exchange mechanisms to address this challenge. The proposed algorithm explores optimal configurations for different energy device placements and capacities through encircling and bubble searches, evaluating various multiobjective functions for optimization. In addition, the algorithm refines both the system operation model and the ESS configuration model, with the objective function being the analysis of the average annual revenue of the ESS. Model testing results demonstrate that this algorithm yields more moderate energy storage (ES) capacity decay, extending operational time to 3,124 days and achieving a full-life cycle benefit of the ESS as high as 1,821,623.68 yuan. Also, our algorithm demonstrates high efficiency, with minimal test time (68.36 seconds) and quick optimization (0.031 seconds per cycle), regardless of problem complexity.

## 1. Introduction

Since the onset of the industrial revolution, the extensive use of fossil fuels such as oil and coal has not only resulted in resource depletion but has also caused significant environmental pollution, thereby subjecting society to the dual pressures of dwindling resources and ecological degradation [1]. Recent years have witnessed the growing adoption of alternative energy sources such as solar power, hydropower, wind energy, and shale gas within active distribution networks [2]. Consequently, issues related to these new energy sources are becoming increasingly salient. Researchers are actively investigating methods for the efficient allocation of ES to mitigate distribution network losses and enhance the effectiveness of renewable energy, ultimately striving to achieve the goals of energy conservation and improved efficiency [3]. However, new energy sources are inherently characterized by randomness, intermittency, and volatility, resulting in considerable fluctuations in the power output of these energy generators and, in turn, introducing challenges in terms of control [4]. The lack of control over new energy power has emerged as a significant constraint hindering the further advancement of this field. In response to the issue of new energy power stability, the integration of ESSs into distribution networks has emerged as a viable solution [5]. Yet, the finite capacity of individual microgrid ESSs poses a challenge. When a substantial volume of renewable energy is introduced, it tends to accelerate the degradation of the ESS's lifespan, leading to increased operational costs for the microgrid [6]. To address this challenge, various types of microgrids located in diverse areas are interconnected to create a comprehensive energy system [7]. This strategy allows for the synchronization of power transmission across these interconnected microgrids, enabling resource sharing

and complementation. An integrated energy system (IES) management strategy not only mitigates the deterioration of ESSs but also enhances their reliability and stability [8]. Such an approach holds the potential to surmount the challenges associated with the widespread adoption of new energy sources.

However, the randomness and volatility of high-density photovoltaic (PV) systems can have a significant impact on the quality of the system voltage waveform, influenced by the external environment [9]. The interference with voltage control equipment's protective mechanisms is a complex issue to manage and regulate, resulting in compromised power quality for consumers and increased network losses. Furthermore, it represents a significant threat to the security and stability of the integrated energy distribution network on the station side. In addition, the uncertainty associated with the distribution of load demand on the consumer side can affect the optimization of the IES [10]. To effectively mitigate the impact of distributed photovoltaics and minimize the influence of consumer power consumption behavior on the system's optimization, ES devices are introduced. These devices rely on more accurate power prediction and operation schedules based on the photovoltaic output and load demand [11]. To optimize the functioning of ES devices and enable the rational utilization of storage batteries and supercapacitors, experts and scholars from around the world have proposed various ideas and achieved notable research outcomes. In literature [12], various methodologies within the Harris hawks optimization (HHO) algorithm are introduced (such as enhanced HHO opposition-based learning (OBL) (EHHOOBL), enhanced HHO Lévy flight (EHHOLF), and enhanced HHO chaotic map (EHHOCM)) aiming to maintain a balance between exploitation and exploration for community detection in social networks. Literature [13] uses the improved African vultures optimization algorithm (AVOA) that uses the three binary thresholds (Kapur's entropy, Tsallis entropy, and Ostu's entropy) in multithreshold image segmentation. The quantum rotation gate (QRG) mechanism has increased population diversity in optimization stages, and optimal local trap escapes to improve AVOA performance. The association strategy (AS) mechanism is used to obtain a faster search for optimal solutions. Literature [14] employs the Harris hawks optimization (HHO) algorithm to propose an innovative technique utilizing random-key encoding for tour generation. This approach preserves the fundamental capabilities of the HHO algorithm while leveraging the functionalities of active mechanisms within the continuous-valued problem space. In the work of literature [15], a novel strategy named MAS as metaheuristic (MAMH) is introduced, incorporating multiagent systems (MASs) and the agent concept. This method treats various potent metaheuristic algorithms as distinct agents, each pursuing individual objectives while concurrently competing and cooperating with others to achieve common goals. Literature [16] enhanced the cuckoo search optimization (CSO) algorithm by integrating a genetic algorithm (GA) for community detection in intricate networks. The GA operators are dynamically employed to enhance the speed and precision of the CSO. The population size is dynamically adapted, balancing exploration and exploitation. The optimization function utilizes the modularity objective function (Q) and normalized mutual information (NMI). To address the issue of local optima entrapment and enhance convergence speed, population-based metaheuristic algorithms are applied. This paper presents an asymmetric clustering approach for the asymmetric self-organizing map, with the interactive autodidactic school (IAS) being among the utilized population-based metaheuristic and asymmetric algorithms [17].

This paper analyzes and investigates the operation efficiency, capacity degradation, and storage lifetime of the ESS with the objective of the average annual return of the IES. Based on the multiobjective whale algorithm, this paper introduces the chaotic mapping and individual information exchange mechanism to overcome the problem of local optimum when solving high-dimensional multiobjective optimization. When studying the optimal operation of the ESS, the installation location and capacity of different energy devices are used as the optimal configuration variables of the algorithm, and then, the optimized whale algorithm is used to solve the optimal configuration of the ESS. Also, the system model is used to verify the effectiveness of its improved algorithm. The paper is organized as follows: the introduction provides an overview of the research, followed by a review of the state of the art. The main body of the algorithm is then presented, along with a comprehensive analysis and discussion of the results. Finally, the study's conclusions are presented in the last section.

## 2. State of the Art

*2.1. Comprehensive Structure of Energy Distribution Network.* Currently, a comprehensive energy distribution network typically comprises various components, including the comprehensive energy system, lithium battery ESS, public power grid, central control unit, and electrical equipment, as depicted in Figure 1.

Within the structure of the comprehensive energy distribution network, we uphold the principle of restricting power supply to electrical equipment through comprehensive energy sources. This strategy significantly curtails the power requirements of electrical equipment from the grid.

*2.2. Application and Optimization Principle of the ESS.* The mathematical model of the integrated energy distribution network is illustrated in Figure 2. This system has the capability to supply multiple forms of energy in the form of heat and power to users. The distribution network encompasses a higher-level grid, an ES device, a photovoltaic power generation system, and a natural engine power generation system. The ESS performs peak shaving and valley filling based on time-sharing tariffs to optimize resource utilization and reduce costs. When the power generated by the new energy generation system exceeds the electrical equipment load, the ES device is charged.

https://doi.org/10.1155/2023/9998972 Published online by Cambridge University Press

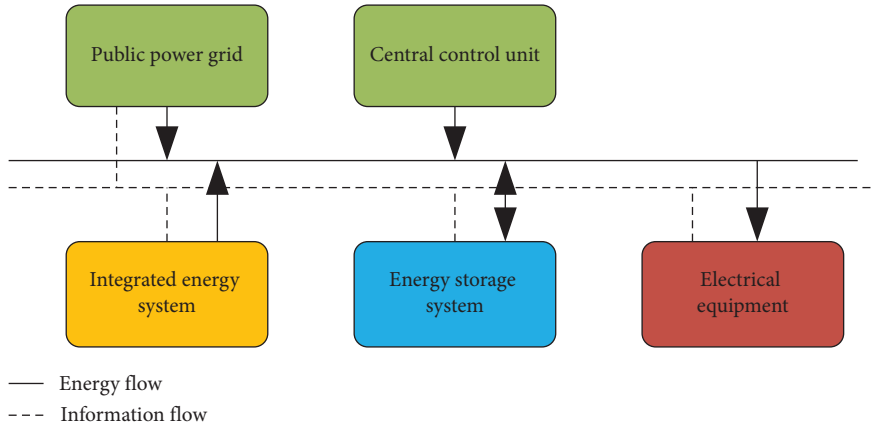


Figure 1: System structure of the integrated energy distribution network.

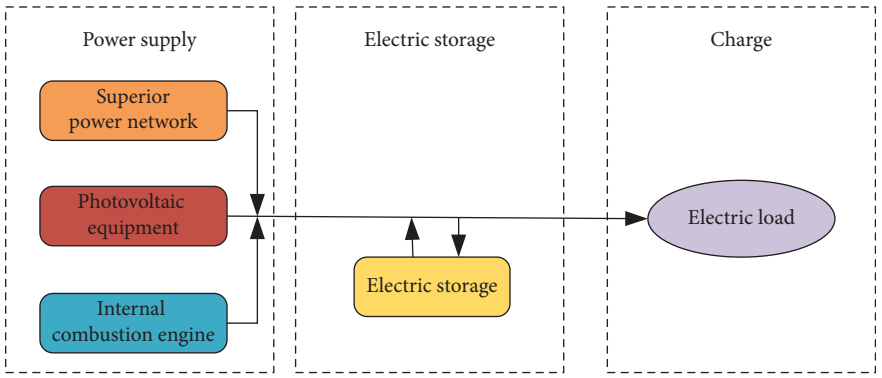


Figure 2: IES structure.

Conversely, when the power is insufficient, the ES device discharges and additional power is procured from the superior grid.

The optimization model of the ESS is depicted in Figure 3. Initially, the output power of the various power supply systems within the IES is regulated in response to the electrical load demand. Subsequently, the system operation model is optimized to identify the most efficient configuration among multiple options for the comprehensive energy system, improving the system's economic performance in the shortest time. Simultaneously, an optimal ES configuration model is developed and the ES capacity is determined based on the output power of different power supply networks and time-of-use (TOU) pricing. As a result, it enhances the annual income of the comprehensive energy system while promoting a slower degradation of ES capacity.

*2.3. Load Analysis of Electrical Equipment.* The electrical equipment represented in the model corresponds to typical high-power household appliances. The key factors influencing the load include the appliance's physical dimensions, initial charging duration, and service duration. Based on findings from a national survey of electrical equipment, the operational time of these appliances follows a log-normal distribution $N(17.8, 3.6)$, as shown in the following equation:

$$f_s(n_1) = \begin{cases} \dfrac{1}{\sigma_s\sqrt{2\pi}} \exp\left[-\dfrac{(n_1-\mu_S)}{2\sigma_s^2}\right], \mu_s - 12 \leqslant n_1 \leqslant 24, \\ \dfrac{1}{\sigma_s\sqrt{2\pi}} \exp\left[-\dfrac{(n_1+24-\mu_s)}{2\sigma_s^2}\right], 0 \leqslant n_1 < \mu_s - 12, \end{cases} \tag{1}$$

where $\mu_s$ and $\sigma_S$ are, respectively, the expected value and standard deviation of the initial charging time of household appliances. $n_1$ is the initial charging time of the electrical device.

Simultaneously, it is assumed that the initial charging time of the electrical equipment follows a uniform distribution, as expressed in the following equation:

$$f_s(n_2) = \text{rand}\ (24, 1), \tag{2}$$

where rand $(24, 1)$ represents the random integer generated in the interval [1, 18]. $n_2$ is the initial charging time of the electrical device.

According to the results of the national survey on electrical equipment, the use time of electrical equipment follows the lognormal distribution $N(45, 0.87)$. Its probability density function is shown in the following equation:

$$f'_D(s_1) = \frac{1}{s_1\sigma_{D_1}\sqrt{2\pi}} \exp\left[\frac{\ln\left(s_1-\mu_{D_1}\right)}{2\sigma_{D_1}}\right], \tag{3}$$

https://doi.org/10.1155/2023/9998972 Published online by Cambridge University Press

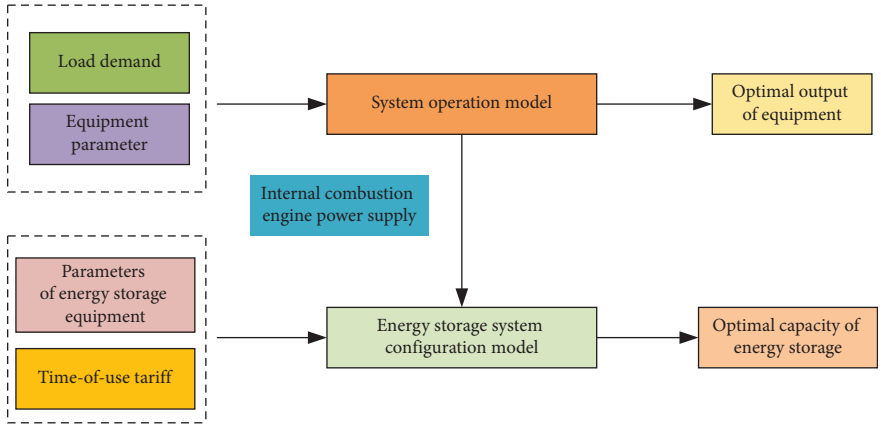


Figure 3: Optimization model structure.

where $\mu_{D_1}$ and $\sigma_{D_1}$ are the expected and standard deviation of the service time of the electrical equipment, respectively. $s_1$ refers to the service duration of electrical devices.

Utilizing the usage guidelines and probability density function provided above, the Monte Carlo algorithm is employed to stochastically sample the initial charging time and service duration of various electrical equipment. Through an analysis of the charging profiles of electrical equipment during different time intervals and the initial state of charge (SOC) of ES batteries, it is possible to subsequently calculate the daily load demand of electrical equipment.

## 3. Methodology

In this paper, the enhanced multiobjective whale optimization algorithm (WOA) [19] is employed in conjunction with models for ES operation efficiency and ES capacity attenuation. This study is focused on addressing ES issues, particularly concerning the efficiency of ES operations and the decline in ES capacity within the ESS. By comparing various algorithms, we investigate differences in ES capacity degradation time, the average annual income of the comprehensive energy system, and system operation efficiency. Furthermore, we delve into the optimization of the ESS using the enhanced algorithm introduced in this paper.

The paper provides a comprehensive methodology for optimizing ESSs through the utilization of the improved WOA. This methodology encompasses enhancements to the algorithm, the management of objective functions, and the modeling of ES efficiency and degradation.

*3.1. Improve the WOA.* The basic WOA is an optimization algorithm based on the behavior of whales to round up prey. It includes the following three search methods: bubble search, enveloping search, and random mutation. Assume that the initial population size of whales is $T$ and the variable dimension is $D$. Cetacean individuals in the solution space position can be expressed as $\overline{I}_x = (i_x^1, i_x^2, \cdots, i_x^D)$. Each whale corresponds to an optimal configuration of the ESS. Upon discovering the optimal individual location, it represents the optimal solution for configuring the ESS.

*3.1.1. Enveloping Search.* Enveloping exploration within the whale optimization algorithm emulates the hunting actions of groups of whales, where the leading whale identifies its target and the other whales employ the lead position as a point of reference. They update their positions in a specific manner to create an encircling pattern around the prey. The equation for individual position updates is provided in the following equation:

$$\begin{cases} \overline{I}(n+1) = \overline{I'}(n) - \overline{G} \cdot \overline{D}, \\ \overline{G} = 2\overline{g} \cdot \overline{r} - \overline{g}, \\ \overline{g} = 2 - \dfrac{2n}{T}, \\ \overline{D} = \left| \overline{C} \cdot \overline{I'}(n) - \overline{I}(n) \right|, \end{cases} \tag{4}$$

where $n$ denotes the present iteration count. $\overline{I}(n+1)$ is the updated position of the individual whale. $\overline{I'}(n)$ is the position of leading whale. $\overline{G}$ is a convergence factor. $\overline{D}$ is the distance between the current individual and the leading whale [20]. $\overline{g}$ linearly diminishes from 2 to 0 with the progression of iterations. $\overline{r}$ and $\overline{C}$ represent random values within the [0, 1] range. $T$ indicates the maximum iteration count.

*3.1.2. Bubble Search.* Bubble search in the algorithm simulates the foraging behavior of whales as they spiral and release bubbles. In this process, individual particles update their positions using the spiral equation, as indicated in the following equation:

$$\overline{I}(n+1) = \overline{D'} \cdot e^{hl} \cdot \cos(2\pi l) + \overline{I'}(n), \tag{5}$$

where $\overline{I}(n+1)$ is the updated position of the individual. $\overline{I'}(n)$ is the leading whale position. $l$ denotes a random number falling within the range of [−1, 1]. $h$ serves as a constant for the spiral path. $D'$ stands for the distance between the current individual and the leading whale.

https://doi.org/10.1155/2023/9998972 Published online by Cambridge University Press

*3.1.3. Random Variation.* Individuals also introduce random changes to their positions as they search for food. This updating mechanism expands the search scope and helps avoid getting stuck in local optimal solutions. The individual position update equation is presented as follows:

$$\begin{cases} \overline{I}(n+1) = \overline{I}_{\text{rand}}(n) - \overline{G} \cdot \overline{D}, \\ \overline{D} = \left| \overline{C} \cdot \overline{I}_{\text{rand}}(n) - \overline{I}(n) \right|, \end{cases} \tag{6}$$

where $\overline{I}(n+1)$ is the updated position of the individual. $\overline{I}_{\text{rand}}(n)$ is the location of a random individual whale.

The improved multiobjective WOA builds upon the basic algorithm, introducing cubic chaotic mapping and an individual information exchange mechanism. In addition, it incorporates a nonlinear convergence factor, adaptive weighting, and multiobjective function processing.

*(1) Initializing the Population Using Cubic Chaotic Mapping.* In the basic WOA, the initial population exhibits high randomness, often starting too far from the optimal solution. This can significantly impede the efficiency of the iterative search. To enhance population diversity and ensure even coverage of the search space, cubic chaotic mapping is employed for dynamic and uniform generation of the initial population. The cubic mapping is expressed in the following equations:

$$\begin{cases} j(t+1) = 4j(t)^3 - 3j(t), \\ -1 < j(t) < 1, j(t) \neq 0, \end{cases} \tag{7}$$

$$i_t = L_d + (1 + j_t)\frac{(U_d - L_d)}{2}, \tag{8}$$

where $U_d$ and $L_d$ are the upper and lower limits of the solution space, respectively. The whale population is generated according to equation (7). The location of the whale is mapped to the solution space according to equation (8) and the location of the whale is initialized.

*(2) Introduce Individual Information Exchange Mechanism.* In the basic WOA, the whale population conducts the search for the optimal solution by updating their positions autonomously. The individual updating mechanism primarily influences the algorithm's iteration efficiency. To enhance the algorithm's convergence rate, the worst solution is updated using a hybrid leapfrog algorithm. An individual information exchange mechanism is introduced to facilitate communication and learning between the weaker individuals and the best individuals. The update equation for the worst solution is provided in the following equation:

$$\overline{I} = \overline{I}_m + r \cdot (\overline{I}_h - \overline{I}_M), \tag{9}$$

where $\overline{I}$ is the updated individual. $\overline{I}_h$ is the best individual in the population. $\overline{I}_M$ is the worst individual. $r$ is a random number between [0, 1].

For the updated individual $\overline{I}$, if $\overline{I}$ is better than $\overline{I}_M$, $\overline{I}$ is used instead of $\overline{I}_M$. Otherwise, substitute $\overline{I}_h$ for $\overline{I}_M$.

*(3) Increase the Nonlinear Convergence Factor and Adaptive Weight.* The search performance of the basic WOA is affected by the convergence factor $G$, and the value of $G$ is determined by $g$. Due to the intricacy of the solution process, the conventional linear degradation approach of a value has proven to be inadequate for addressing real-world engineering needs, particularly in high-dimensional nonlinear optimization problems. As a result, this paper introduces an updated method for the traditional convergence factor, and its calculation equation is presented as follows:

$$g(n) = 2 - u_1 \cdot e^{u_2 \cdot n / N_{\max}}. \tag{10}$$

In the equation, $u_1$ and $u_2$ are nonlinear adjustment parameters and the values in this paper are 0.07 and $9/8\pi$, respectively.

In the optimization process of the WOA, a balance must be struck between the convergence efficiency and the algorithm's solution precision. During the initial optimization stages, the range of random search is expanded to prevent getting trapped in local optima. In the later stages of optimization, it is essential to enhance the learning capability of the optimal solution to accelerate algorithm convergence. Therefore, an adaptive weight coefficient is introduced to balance the global and local search abilities of the algorithm. After introducing this new convergence factor, equations (4)–(6) are updated as shown in the following equation:

$$\begin{cases} \overline{I}(n+1) = g(n) \cdot I_h(n) - G \cdot D, \\ \overline{I}(n+1) = g(n) \cdot I_h(n) + D \cdot e^{hl} \cos(2\pi l), \\ \overline{I}(n+1) = [1 - g(n)] \cdot I_{\text{rand}}(n) - G \cdot D. \end{cases} \tag{11}$$

*(4) Multiobjective Function Processing.* To address the optimal configuration model of the multiobjective function proposed in this paper, the basic WOA is enhanced in the following two aspects.

(1) A fast nondominant sort is introduced to calculate the crowding degree and the elite retention strategy.

(2) Choose the solution with the highest comprehensive satisfaction based on information entropy. The specific steps are as follows.

Step 1: Normalize the objective function. The calculation method is shown in the following equation:

$$\mu_{x,z} = \frac{f_{x,\max} - f_{x,z}}{f_{x,z} - f_{x,\min}}, \tag{12}$$

where $f_{x,z}$ is the actual value of the $k$-th objective function of individual $x$. $\mu_{x,z}$ is the value after normalization of the $k$-th objective function of individual $x$. $f_{x,\max}$ is the maximum value of the $k$-th objective function of individual $x$. $f_{x,\min}$ is its minimum value.

Step 2: Calculate the weight of each indicator. The expression is shown in the following equation:

https://doi.org/10.1155/2023/9998972 Published online by Cambridge University Press

$$\begin{cases} M_z = -\dfrac{1}{\ln\ (t)} \displaystyle\sum_{x=1}^{t} \left( \dfrac{\mu_{x,z}}{\sum_{x=1}^{t} \mu_{x,z}} \cdot \ln\ \dfrac{\mu_{x,z}}{\sum_{x=1}^{t} \mu_{x,z}} \right), \\ \tau_z = \dfrac{1 - M_z}{t - \sum_{x=1}^{t} M_z}, \end{cases} \tag{13}$$

where $M_z$ is the information entropy of the $k$-th attribute. $\tau_z$ is the weight of the $k$-th attribute.

Step 3: Calculate the scale and fit degree, as shown in the following equation:

$$\begin{cases} S_{x,+} = \sqrt{\displaystyle\sum_{z=1}^{w} \left( \tau_z \mu_{x,z} - \tau_z \mu_{x,z+} \right)^2}, \\ S_{x,-} = \sqrt{\displaystyle\sum_{z=1}^{w} \left( \tau_z \mu_{x,z} - \tau_z \mu_{x,z-} \right)^2}, \\ C_x = \dfrac{S_{x,-}}{S_{x,-} + S_{x,+}}, \end{cases} \tag{14}$$

where $S_{x,+}$ and $S_{x,-}$ are the positive ideal distance and negative ideal distance of individual $x$, respectively. $\mu_{x,z+}$ is the maximum value of all objective functions of individual $x$ after normalization. $\mu_{x,z-}$ is its minimum value. $C_x$ is the fit degree of individual $x$, and the larger the value, the higher the comprehensive satisfaction of the solution.

Step 4: Choose the solution with the highest $C_x$ value as the compromise solution.

In the multiobjective optimal configuration model proposed in this algorithm, the variables to be optimized are the installation position and capacity of the ESS. The improved WOA simulates the spatial positions of whale groups. The initialization of the whale population's locations corresponds to the initialization of numerous ES configurations. The whale population continuously updates its positions through enveloping search, bubble search, random variation, and individual communication until it discovers the optimal solution. This process is equivalent to comparing and optimizing multiple objective functions associated with various configuration schemes. The optimal positions of the whales represent the optimal allocation of ES. The solution steps using the enhanced WOA are outlined as follows.

(1) Input the power supply, load timing output parameters, and algorithm-related parameters.

(2) Initialize the whale population using cubic chaotic mapping. Then, calculate the objective function values for each whale in the population.

(3) Perform rapid nondominant sorting of the whale individuals in the algorithm.

(4) Utilize the enhanced WOA to update and optimize the positions of each individual whale.

(5) Check whether the optimization process has reached the maximum number of iterations. If not, return to step (2). If the maximum iterations are reached, output the set of frontier solutions.

(6) Select the compromise solution based on the normalized processing values and output the final optimal configuration scheme.

The algorithm flowchart of this paper is shown in Figure 4.

The time complexity of the algorithm can be summarized as follows. The input parameter step (step 1) has a constant time complexity $O(1)$. The population initialization and objective function evaluation step (step 2) have a time complexity of $O(N + K * N)$, where $N$ is the population size and $K$ is the number of objective functions. The fast nondominant sorting step (step 3) has a time complexity of $O(N^2)$, where $N$ is the population size. The update and optimization of individual positions step (step 4) have a time complexity of $O(N)$. The termination condition check step (step 5) has a constant time complexity $O(1)$. Lastly, the compromise solution selection step (step 6) has a time complexity of $O(K * N)$, where $K$ is the number of objective functions and $N$ is the population size. Overall, the entire algorithm's time complexity is $O(N^2 + K * N)$.

### 3.2. Construction of the ES Model

#### 3.2.1. Constraints

*(1) Power-Balance Constraints*

$$U_{\mathrm{sol},n} + U_{s,n} = U_{v,n} + U_{\mathrm{grid},n}, \tag{15}$$

where $U_{\mathrm{sol},n}$ is the output of the IES at time $n$. $U_{s,n}$ is the output of the ESS in time cycle $n$. This paper assumes that $U_{s,n}$ remains constant over time $n$. $U_{v,n}$ indicates the total power required by the charging device during time $n$. $U_{\mathrm{grid},n}$ is the power traded between the IES and the grid during $n$ cycle.

*(2) ES Constraints*

(a) The maximum and minimum limits of ES output are shown in the following equation:

$$-U_{s,\max} \leqslant U_{s,n} \leqslant U_{s,\max}, \tag{16}$$

where $U_{s,\max}$ is the maximum output of the ESS.

(b) The following equation illustrates the SOC constraints for energy storage.

$$K_{\mathrm{soc}}^{\min,n} \leqslant K_{\mathrm{soc}}^{n} \leqslant K_{\mathrm{soc}}^{\max,n}, \tag{17}$$

where $K_{\mathrm{soc}}^{n}$ is the SOC of the ESS during cycle $n$. $K_{\mathrm{soc}}^{\min,n}$ and $K_{\mathrm{soc}}^{\max,n}$ are the minimum and maximum SOC of the ESS in time cycle $n$, respectively.

https://doi.org/10.1155/2023/9998972 Published online by Cambridge University Press

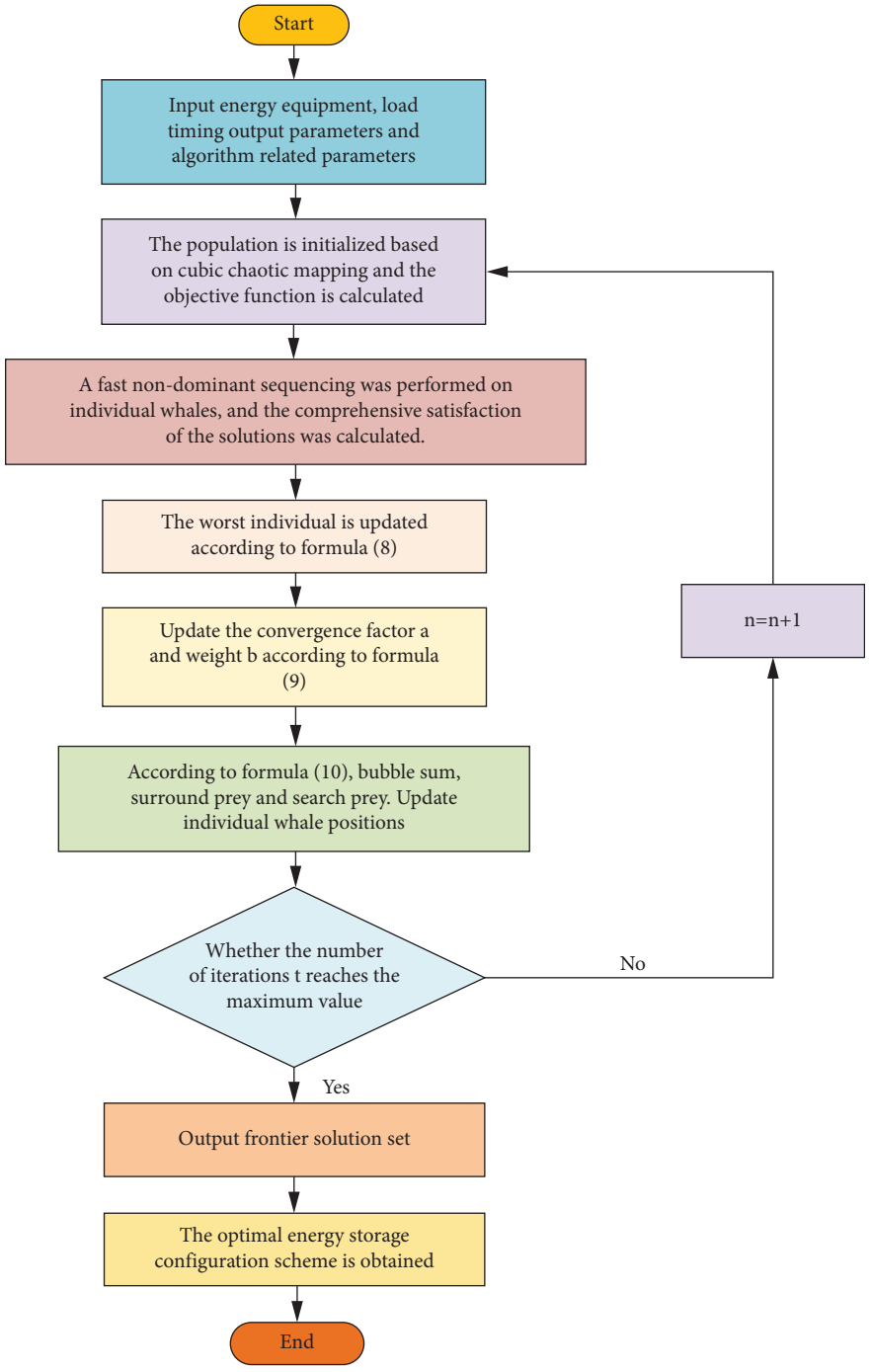


Figure 4: The algorithm flowchart of this paper.

The SOC conversion of ES battery is given by the following equation:

$$K_{\text{soc}}^{n+1} = \begin{cases} K_{\text{soc}}^{n} - \eta_n^c \dfrac{U_{s,n}\Delta n}{F_{ini}}, & U_{s,n} \leqslant 0, \\ K_{\text{soc}}^{n} - \dfrac{1}{\eta_n^{\text{disc}}} \dfrac{U_{s,n}\Delta n}{F_{ini}}, & U_{s,n} > 0, \end{cases} \tag{18}$$

where $\eta_n^c$ is the charging efficiency of the ES battery in time cycle $n$. $\eta_n^{\text{disc}}$ is the discharge efficiency of the ES battery during this cycle [21].

(c) SOC constraints in the final cycle of ESS.

To guarantee the proper functioning of the ESS in the subsequent control cycle, the SOC after the ES action in the preceding cycle needs to be adjusted to a predefined value. The calculation equation for this adjustment is provided in the following equation:

https://doi.org/10.1155/2023/9998972 Published online by Cambridge University Press

$$K_{\text{soc}}^{N_o+1} = K_{\text{soc}}^{1}. \tag{19}$$

$N_o$ is the cycle number. In this article, a cycle is 1 day and there are 96 cycles.

(d) SOC penalty at the conclusion of the ES cycle.

According to the constraint condition (19), the SOC penalty in the final cycle of ES is shown in the following equation:

$$r_{n,4} = \begin{cases} \left|K_{\text{soc}}^{N_0+1} - K_{\text{soc}}^{1}\right|, & n = N_0, \\ 0, & n < N_0, \end{cases} \tag{20}$$

where $r_{n,4}$ signifies the SOC without penalty in the final cycle of ES.

In summary, the reward and penalty function is articulated as in the following equation:

$$r_n = \sigma_1 r_{n,1} - \sigma_2 r_{n,2} - \sigma_3 r_{n,3} - \sigma_4 r_{n,4}, \tag{21}$$

where $r_n$ is the immediate return at time cycle $n$. $\sigma_1, \sigma_2, \sigma_3$, and $\sigma_4$ are the weight coefficients of each component of the reward and penalty, and all are positive. They are in the range [0, 20] and are chosen as $\sigma_1 = 10$, $\sigma_2 = 13.5$, $\sigma_3 = 15$, $\sigma_4 = 18.5$, respectively.

*3.2.2. Operation Efficiency Model of ES.* The efficiency of battery charging and discharging can be ascertained by employing the steady-state circuit equivalent model of the battery [22], as shown in Figure 5.

$V_{oc}$ is the open-circuit voltage in the figure. $I_b$ indicates the battery current. $U_{\text{out}}$ indicates the output power. $R_1$ is the series resistance. $R_2$ is a short-time response resistance associated with transient response. $R_3$ represents a short-time response resistor linked to transient response, as well as a long-time response resistor. All the aforementioned variables exhibit a nonlinear relationship with the battery's SOC, as demonstrated in the following equation:

$$\begin{cases} V_{oc} = a_0 f^{-a_1 k_{\text{soc}}} + a_2 + a_3 K_{\text{soc}} - a_4 K_{\text{soc}}^2 + a_5 K_{\text{soc}}^3, \\ R_1 = h_0 f^{-h_1 K_{\text{soc}}} + h_2 + h_3 K_{\text{soc}} - h_4 K_{\text{soc}}^2 + h_5 K_{\text{soc}}^3, \\ R_2 = c_0 f^{-m_1 K_{\text{soc}}} + m_2, \\ R_3 = d_0 f^{-n_1 K_{\text{soc}}} + n_2, \\ R_t = R_1 + R_2 + R_3, \end{cases} \tag{22}$$

where $R_t$ is the terminal resistance. $a_0$-$a_5$, $h_0$-$h_5$, $m_0$-$m_2$, and $n_0$-$n_2$ are all coefficients.

By solving equation (23) for a given SOC and $U_{\text{out}}$, the current through an individual cell can be determined.

$$I_b^2 R_t - I_b V_{oc} + U_{\text{out}} = 0. \tag{23}$$

The following equation conveys the charging and discharging efficacy of an individual battery.

$$\begin{cases} \eta^c = \dfrac{V_{oc}}{V_{oc} - I_b R_t}, \\ \eta^{\text{disc}} = \dfrac{V_{oc} - I_b R_t}{V_{oc}}, \end{cases} \tag{24}$$

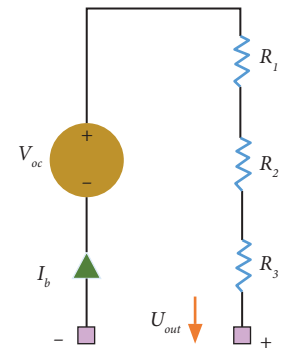


Figure 5: Steady-state circuit equivalent model.

where $\eta^c$ and $\eta^{\text{disc}}$ represent the charging and discharging efficiency of the battery, respectively.

The energy storage system (ESS) utilized in this study comprises numerous batteries organized in both series and parallel configurations. The following equations offer the formulas for calculating the charging and discharging efficiencies of the equivalent current, respectively.

$$I_e^2 R_t - I V_{oc} + U_{es} \frac{1}{T_{\text{series}} T_{\text{para}}} = 0, \tag{25}$$

$$\begin{cases} \eta^c = \dfrac{V_{oc}}{V_{oc} - I_e R_t}, \\ \eta^{\text{disc}} = \dfrac{V_{oc} - I_e R_t}{V_{oc}}, \end{cases} \tag{26}$$

where $I_e$ represents the electric current of the ES battery. $I$ denotes the total current considering multiple batteries arranged in both series and parallel configurations. $T_{\text{series}} i$ indicates the count of battery cells arranged in series, while $T_{\text{para}}$ represents the number of battery units linked in parallel. $U_{es}$ is the ES battery power.

The operational efficiency was computed using equation (26). The correlation between operational efficiency and output power and SOC was modeled using a second-order polynomial, as demonstrated in the following equation:

$$\begin{cases} \eta^c = f_0 + f_1 K_{\text{soc}} + f_2 K_{\text{soc}}^2 + f_3 U_{es} + f_4 U_{es}^2 + f_5 U_{es} K_{\text{soc}}, \\ \eta^{1/\text{disc}} = b_0 + b_1 K_{\text{soc}} + b_2 K_{\text{soc}}^2 + b_3 U_{es} + b_4 U_{es}^2 + b_5 U_{es} K_{\text{soc}}. \end{cases} \tag{27}$$

In the equation, $f_0$-$f_5$ and $b_0$-$b_5$ denote the coefficients.

*3.2.3. ES Attenuation Model.* Battery capacity degradation is influenced by ambient temperature, depth of discharge, SOC, and battery runtime. It is a nonlinear process and not a simple sum of individual cycle degradation. This paper employs a semiempirical battery capacity degradation model. Over $T$ loops, the battery-capacity degradation model is defined in the following equation:

$$F_{\text{loss}} = \begin{cases} \left[1 - \mu_{\text{sei}} f^{-T\gamma_{\text{sei}} l_d} - (1 - \mu_{\text{sei}}) f^{-Tl_d}\right] F_{\text{ini}}, & F'_{\text{loss}} = 0, \\ \left[1 - (1 - F'_{\text{loss}}) f^{-Tl_d}\right] F_{\text{ini}}, & F'_{\text{loss}} > 0, \end{cases} \tag{28}$$

https://doi.org/10.1155/2023/9998972 Published online by Cambridge University Press

where $F'_{\text{loss}}$ and $F_{\text{loss}}$ denote the decay capacities before and after $T$ loops, respectively. If $F'_{\text{loss}} = 0$, it indicates that the battery has not undergone charging or discharging processes. $\mu_{\text{sei}}$ and $\gamma_{\text{sei}}$ are the influencing factors for solid electrolyte interface (SEI) membrane formation during the use of new batteries. $l_d$ is the capacity attenuation function of a single cycle.

The residual usable capacity $F_r$ of the ES battery is shown in the following equation:

$$F_r = F_{\text{ini}} - F_{\text{loss}}, \tag{29}$$

where $F_{\text{ini}}$ is the maximum capacity of the ES battery before attenuation. $F_{\text{loss}}$ is the discharge capacity of the ES battery.

Equations (28) and (29) represent the approach for calculating battery capacity degradation. However, obtaining parameters for each cycle can be challenging in practice because battery charge and discharge patterns are often irregular. To address this, the rain-flow counting method is utilized to compute battery loops and their associated parameters [23]. Figure 6 illustrates the process of calculating ES battery capacity degradation using this method.

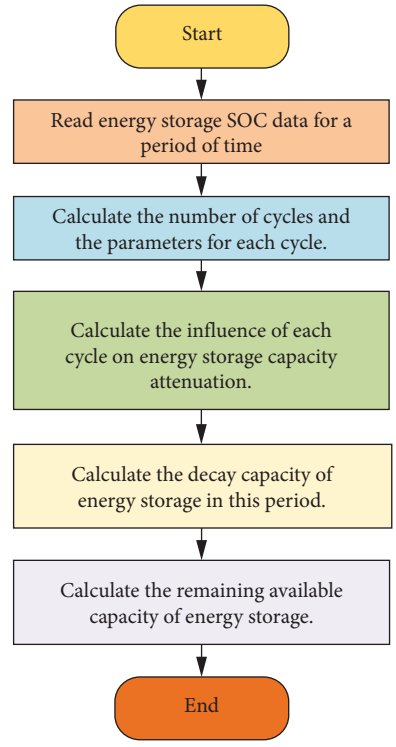


Figure 6: Calculation flow of ES battery capacity attenuation.

## 4. Result Analysis and Discussion

This paper has established a comprehensive ESS model, encompassing the system operation model and the ES decay model. By optimizing these models, the average annual revenue status of the ESS is determined. The effectiveness of the algorithms and models proposed in this paper is demonstrated through comparisons and analyses with other approaches. The abstract underscores the importance of optimizing ESS capacity allocation to address the volatility and uncontrollability of renewable energy generation for energy stability. Given regional constraints, seasonal variations, and mid-day climate impacting photovoltaic energy systems, this paper indirectly derives the optimal capacity and power solution through the average annual return profile of the ESS.

740 arrays of photovoltaic cells are utilized in this investigation, collectively possessing an ES capacity of 14.10 MW. When the capacity of 1949 storage batteries declines to 80% of their designated capacity, they are no longer deemed functional. The ESS operates at a charging and discharging efficiency rate of 90%. The overall system cost is approximately 32.8 million yuan, and the time-of-use electricity prices are detailed in Table 1.

In this paper, three comparative algorithms are selected, and their specific details are presented in Table 2. During testing, each algorithm's specific test conditions and parameters are described in Figure 7. For their proposed algorithm, the authors likely conducted experiments or simulations to determine the optimal parameter values. The sensitivity of these parameters to the performance of the proposed algorithm is of utmost importance in ensuring its effectiveness. Initially, the fitness function weights are set by assigning suitable weights to each objective. Altering these weights enables the algorithm to discover optimal solutions. Subsequently, termination criteria are defined. These criteria dictate when the algorithm should cease iterations. By setting a maximum number of iterations or a convergence threshold, the algorithm's convergence is enhanced, and excessive computations are avoided. Evaluating the algorithm's performance involves individually or collectively varying these parameters to identify their optimal values. This process aids in understanding how parameter changes impact the algorithm's behavior, facilitating fine tuning for improved performance.

When the algorithm in this paper uses the actual data for training, only the current cycle data are obtained in the test stage and the loss of the ESS is considered. Literature [24] addresses the ESS charging and discharging approach under theoretical conditions, assuming all the factual information. In contrast, literature [18] utilizes "actual data +17% deviation data within a normal distribution" during the training phase, introducing variations between the data and the factual information. In order to verify the robustness of the calculation, the method considers many uncertain factors such as comprehensive energy, electrical equipment charging, and electricity price. Literature [25] also assumes that the charging and discharging strategy of the ESS is solved when the actual data is known, but the loss of ES is not considered. Since the proposed algorithm converts all costs of ES, the average annual income is taken as the standard to judge the optimization effect.

Table 3 shows the benefits of ESS calculated by different algorithms. Figure 8 shows their corresponding ES capacity attenuation curves.

The results presented in Table 3 indicate that the ESS operated by the algorithm in this paper has a duration of 3,124 days, which is the longest among the compared algorithms. Moreover, it yields the highest life cycle benefit for the ESS. The average annual income from this algorithm

https://doi.org/10.1155/2023/9998972 Published online by Cambridge University Press

Table 1: The time-of-use electricity prices used in the simulation case.

| Highest peaks and lowest valleys | | | | |
|---|---|---|---|---|
| Time cycle | 19:00–22:00 | 8:00–11:00<br>15:00–19:00 | 7:00-8:00<br>11:00–15:00<br>22:00-23:00 | 23:00–7:00 |
| Commercial electricity price/yuan/kW·h | 0.98 | 0.88 | 0.65 | 0.44 |
| Industrial electricity price/yuan/kW h | 0.93 | 0.85 | 0.58 | 0.41 |

Table 2: Description of the proposed algorithm and the referenced algorithm.

| Methods | Descriptions of the algorithms |
|---|---|
| Literature [24] | Basic whale algorithm |
| Literature [18] | NSGA-II |
| Literature [25] | Improved whale algorithm with NSGA-II |
| Proposed | Multiobjective whale algorithm introducing chaotic mapping and individual information exchange mechanism |

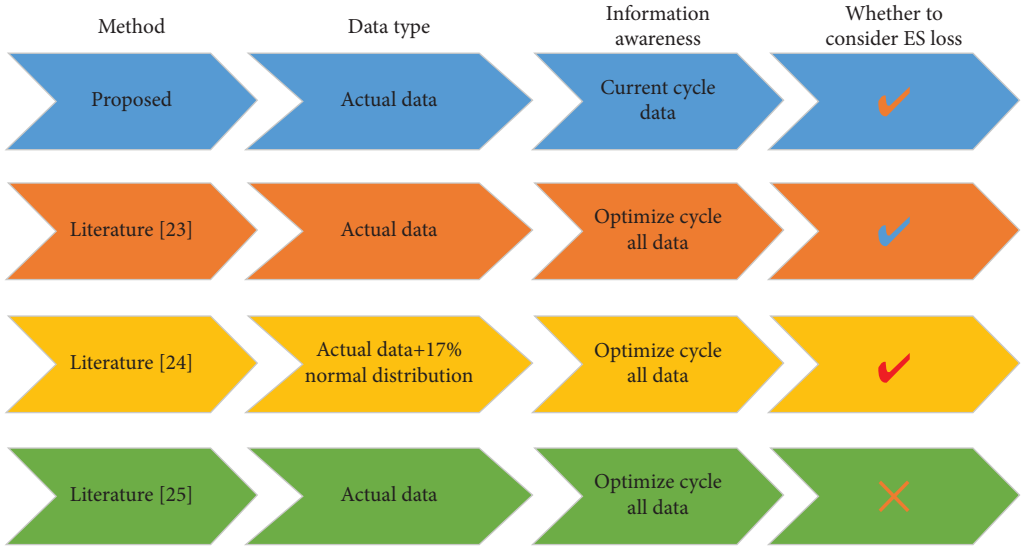


Figure 7: Comparison of the four methods.

Table 3: Revenues of the photovoltaic-storage charging station.

| Methods | ES life (day) | Life cycle revenue (yuan) | Average annual revenue (yuan·a$^{-1}$) |
|---|---|---|---|
| Proposed | 3124 | 1821623.68 | 199728.51 |
| Literature [24] | 2274 | 1489288.73 | 223105.39 |
| Literature [18] | 1885 | 1033258.44 | 186378.87 |
| Literature [25] | 1314 | 659334.72 | 168685.76 |

ranks second, with only literature [24] outperforming it. However, it is worth noting that literature [24] achieves the best optimization results because it considers an ideal scenario where it already knows the actual data of all cycles in advance when optimizing. While this approach results in the highest average annual return, it necessitates having access to actual data within the optimization cycle, which might not be practical in real-world applications. The algorithm in this paper operates under more realistic conditions, considering only current data during testing, which may explain the difference in performance.

In comparison to literature [24], literature [18] uses more data than the actual data. Specifically, it adds extra 17% deviation data based on the actual data, with these data following a normal distribution. This approach results in a notable reduction in the lifespan of the ESS, as well as a decrease in the system's life cycle income and annual average income. However, when compared to the algorithm presented in this paper, the average annual return from literature [18] is only slightly lower. This comparison highlights that the proposed algorithm can effectively address the charging and discharging decision problem of an

https://doi.org/10.1155/2023/9998972 Published online by Cambridge University Press

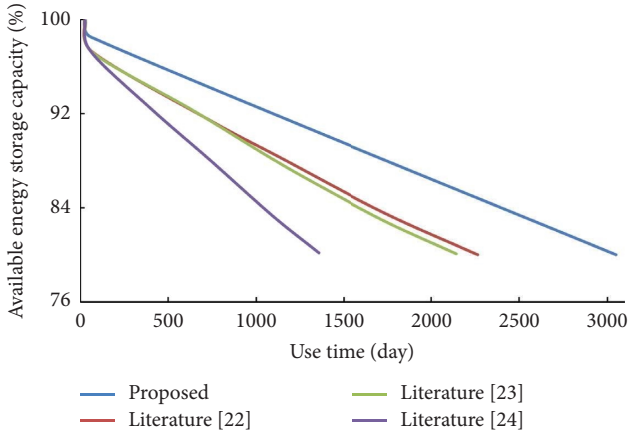


Figure 8: ES capacity attenuation curve.

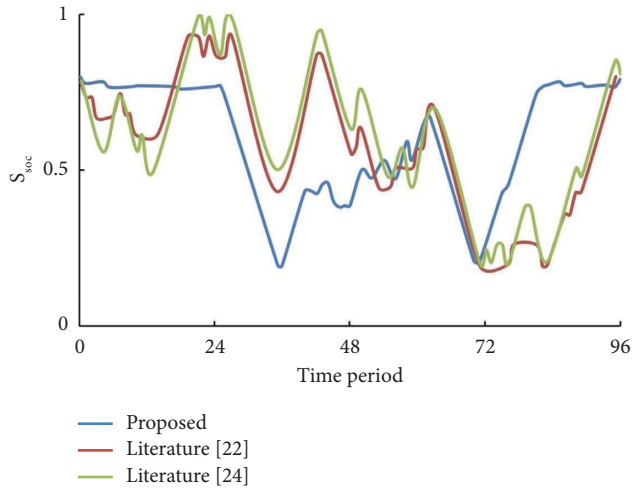


Figure 9: SOC of energy storage.

ESS in an uncertain environment, offering competitive results. It suggests that the algorithm's ability to optimize ESS performance even in the face of uncertainties makes it a valuable tool for practical applications.

The analysis of Figure 8 reveals that when not considering energy action losses, the ESS optimized by literature [18] has the shortest lifespan at 1314 days. This is because literature [18] does not account for energy action losses. In comparison, literature [24] uses data with an additional 17% normal distribution bias, leading to a reduction of 389 days in the lifespan of the ESS when compared to literature [23]. In contrast to literature [23], which optimizes the entire cycle of data, the algorithm presented in this paper utilizes data from the current time cycle, resulting in the longest lifespan for the system. This surpasses the performance of literature [23] by 850 days. Thus, it can be inferred that energy capacity losses, which lead to frequent charging and discharging of the ESS, accelerate the decay of its lifespan and ultimately reduce its long-term benefits. This demonstrates the importance of considering energy action losses in optimizing ESSs, as our algorithm achieves the longest system lifespan, highlighting its effectiveness.

Absolutely, we have made a succinct and accurate observation. ES capacity loss indeed leads to frequent charge and discharge loops of the ESS. This accelerated cycling of ES components can significantly reduce the overall lifespan of the system and, consequently, diminish the long-term benefits it provides. This insight underscores the importance of considering and mitigating ES capacity decay in the design and optimization of ESSs to ensure their sustained effectiveness.

The test result of energy storage SOC on a certain day is shown in Figure 9. The proposed algorithm can discharge the ESS when the electricity price is high and charge it when the electricity price is low. This shows that the improved algorithm in this paper can learn the scheduling strategy that makes the return higher. Compared to literature [18], literatures [23, 24] reduce the number of charging and discharging loops, resulting in lower power for these operations. In comparison to literatures [18, 23], our algorithm achieves the least number of charging and discharging loops for the ESS. This is because in our algorithm, we assign a higher weight coefficient to the cost of ES, which extends the lifespan of the system. During the decision-making stage, our algorithm sacrifices short-term benefits by reducing immediate gains in order to accumulate long-term benefits.

In this case, $\sigma_2$ relating to the ESS's capacity reduction penalty is utilized to delve deeper into the impact of the weight coefficient on the outcomes of the reinforcement learning algorithm. The statistical results of sensitivity analysis with the weight coefficient $\sigma_2$ are shown in Table 4.

The analysis in Table 4 shows that with the increase of $\sigma_2$, the life of the ESS extends. At the same time, the life cycle returns also increase. When $\sigma_2$ is less than 5, the average annual revenue of the ESS increases. This indicates that the choice of actions is more likely to avoid the end of the ES penalty. As $\sigma_2$ increases, the way in which ES can be acted and profited from becomes more rational. However, when $\sigma_2$ is greater than 5, the average annual revenue of the ESS begins to decrease and the decrease amplitude gradually increases. This indicates that the ESS prioritizes the effects of capacity reduction from ES actions when forming judgments. As $\sigma_2$ increases, the ESS reduces the number of ES operations to delay capacity decay. As a result, prolonged operational longevity and increased overall life cycle advantages can be achieved.

The parameters utilized in the algorithm simulation within this study, like $\sigma_2$, were determined after numerous trial simulations to derive a set of comparatively superior experimental parameters. Nevertheless, this set of trial parameters might not represent the most optimal, highlighting the challenge of parameter adjustment in the whale algorithm. From Table 5, it can be observed that our algorithm requires the longest time during training, but it operates faster in the testing phase after the model is trained, with an average optimization time of 0.0031 s per cycle. The time taken to test our algorithm is 68.36 seconds, and the optimization duration per cycle is independent of the issue's intricacy. The other three algorithms do not require pretraining, so their training time is 0 s. Since they assume a constant operating efficiency for the ESS, they all require

https://doi.org/10.1155/2023/9998972 Published online by Cambridge University Press

Table 4: Sensitivity review of the weight coefficient $\sigma_2$.

| $\sigma_2$ | ES life (day) | Life cycle revenue (yuan) | Average annual revenue (yuan·a$^{-1}$) |
|---|---|---|---|
| 1.5 | 1588 | 682858.61 | 155256.84 |
| 3 | 2721 | 1523658.75 | 188756.67 |
| 6 | 3154 | 1773482.24 | 213862.48 |
| 9 | 3526 | 1856936.51 | 199858.22 |
| 15 | 6313 | 2716388.35 | 163252.73 |

Table 5: Comparative analysis of computation time among the four algorithms.

| Methods | Training time (s) | Test time (s) | Average optimization time of each cycle (s) |
|---|---|---|---|
| Proposed | 9284 | 68.36 | 0.0031 |
| Literature [24] | 0 | 33656.74 | 0.1514 |
| Literature [18] | 0 | 26569.35 | 0.1623 |
| Literature [25] | 0 | 1286.72 | 0.02115 |

longer testing time compared to our algorithm. Literature [23] has the longest testing time, while literature [24] has the longest average optimization time per time cycle. Due to the fact that literature [18] does not consider the degradation of the ESS, its average optimization time per time cycle is less than that of literature [23] and literature [24]. However, it still requires more time compared to our algorithm. This indicates that our improved algorithm maintains a higher computational efficiency in complex problems.

The iterative convergence curves of the proposed, literature [26], and literature [27] are shown in Figure 10. It can be seen from Figure 9 that under the same population size and the same number of iterations, the objective functions of the three algorithms decrease with the increase of iterations. However, the convergence speed of the proposed algorithm is fast, which reduces the risk of premature convergence of particles. This shows that the proposed algorithm has strong global and local search ability and faster convergence speed.

In order to provide empirical evidence supporting the significant improvement advantages of the improved algorithm proposed in this paper over other existing algorithms, a Wilcoxon rank-sum test [28] was conducted independently to compare the results of each experiment at a significance level of 5%. The comparison results are presented in Table 6, where "$p$" represents the test result and "$h$" indicates the significance judgment result. If "$p$" is less than 0.05, "$h$" is denoted as 1, which means the significance of this algorithm is stronger than other algorithms. Conversely, if "$p$" is greater than 0.05, "$h$" is denoted as 0, indicating that the significance of this algorithm is weaker than other algorithms. In cases where "$p$" is displayed as N/A, it indicates

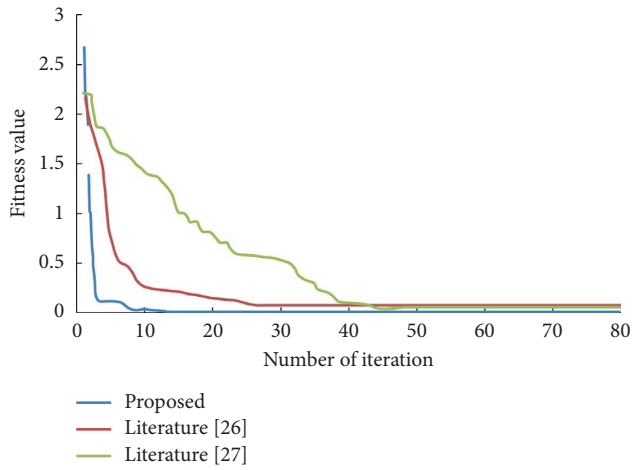


Figure 10: Fitness convergence curve.

that a significance test could not be performed and the significance of the proposed algorithm may be similar to that of other algorithms. Based on the statistical results presented in Table 6, it is evident that the majority of the $p$ values are below the significance level of 0.05. This compellingly indicates that there exist significant differences between the proposed algorithm and other algorithms under comparison. Notably, the performance of the proposed algorithm consistently outperforms the comparison algorithms across various functions. These findings strongly support the effectiveness and superiority of the proposed approach, lending further credibility to its potential for improved performance and applicability.

https://doi.org/10.1155/2023/9998972 Published online by Cambridge University Press

Table 6: Results of the Wilcoxon rank-sum test.

| Functions | Proposed | | Literature [25] | | Literature [26] | | Literature [27] | |
|---|---|---|---|---|---|---|---|---|
| | $p$ | $h$ | $p$ | $h$ | $p$ | $h$ | $p$ | $h$ |
| Sphere [29] | $1.27E-05$ | 1 | $1.21E-12$ | 1 | $8.86E-07$ | 1 | $1.21E-12$ | 1 |
| Quartic [30] | $1.33E-05$ | 1 | $1.21E-12$ | 1 | $4.46E-06$ | 1 | $2.39E-11$ | 1 |
| Rastrigin [31] | N/A | 0 | $1.21E-12$ | 1 | N/A | 0 | $1.21E-12$ | 1 |

## 5. Conclusions and Future Works

Addressing the capacity degradation and operational efficiency optimization problem in IESs, this paper utilizes an enhanced WOA. The experimental model takes into account the uncertainty associated with photovoltaic power generation, electric appliance charging loads, and electricity prices. In comparison to literatures [18, 23, 24], this paper's algorithm exhibits certain advantages. First, it avoids directly modeling uncertainties, reducing the impact of variations in the power output and electric device charging demands within IESs, while also overcoming uncertainties related to electricity prices on optimization results. Second, it does not require access to actual data for future time cycles to achieve relatively optimal results, thus reducing the influence of forecasting errors on the optimization outcome. Experimental results indicate that this paper's algorithm can overcome issues of multiobjective optimization being susceptible to local optima. It effectively enhances ES capacity degradation, resulting in extended lifespans and higher overall lifecycle returns for ESSs. Moreover, the algorithm optimizes the operation of ES devices, increasing the economic viability of ESSs. However, this paper considers the charging demands of all electrical appliances as a whole and does not categorize the charging devices or account for their spatial distribution. Therefore, this algorithm is not suited for studying the charging strategies of individual devices or optimizing the spatial distribution of charging devices. A future research direction may involve a finer analysis of the spatiotemporal distribution of electrical appliances, optimizing their charging strategies and considering voltage deviations and investment costs. The paper's abstract mentions one of its objectives as improving the optimal installation positions and capacities of various energy devices. However, specific optimization details are not disclosed in this paper. Future research may further explore and reveal these optimization details.

Aiming at the optimization problem of capacity attenuation and operation efficiency of ESS in IES, this paper adopts the improved whale algorithm to solve the problem. The experimental model fully considers the uncertainties of photovoltaic power generation, charging load of electrical equipment, and electricity price. Compared with the literatures [18, 23, 24], the algorithm in this paper has certain advantages. One is that it avoids direct modeling of uncertainty, which reduces the power issued by the IES and the charging demand of electric devices, while overcoming the impact of uncertainties such as electricity price on the optimization results. Second, it can get better results without obtaining the actual data in the future time cycle, which reduces the impact of the prediction error on the optimization results. Experimental results show that the algorithm in this paper can overcome the problem of multiobjective optimization, which is easy to fall into the local optimum, and effectively improve the ES capacity degradation so that the ES device can obtain a longer operating life and higher whole-life cycle revenue. At the same time, the algorithm in this paper optimizes the working process of the ES device, which increases the economy of the ESS. However, this paper considers the charging demand of all electrical devices as a whole and does not categorize the charging devices or consider the spatial distribution of charging devices. The algorithm in this paper cannot be used to study the charging strategy for each piece of equipment and the charging strategy optimized for the spatial distribution of charging equipment. Further refinement to the spatial and temporal distribution of electrical equipment, optimization of its charging strategy, while taking into account the voltage deviation and investment costs will be the direction of the subsequent research. In the abstract part of the paper, it is mentioned that one of the objectives of this paper is to improve the optimal location and capacity of various energy devices. However, for some reasons, specific optimization details are not revealed in this paper. Future research may further explore and reveal these optimization details.

## Data Availability

The datasets used to support the findings of this study are available from the corresponding author upon request.

## Conflicts of Interest

The authors declare that there are no conflicts of interest.

## Acknowledgments

This work was supported by the 2023 Henan Province Key Research and Development (R&D) and Promotion Special (Science and Technology Research) Project, Project no. 232102210201, Project Name: 5G+Cloud VR Application in Remote Visiting Systems.

## References

[1] A. M. Idris, N. A. Sasongko, and Y. D. Kuntjoro, "Energy conversion and conservation Technology in facing net zero-emission conditions and supporting national defense," *Trends in Renewable Energy*, vol. 8, no. 1, pp. 49–66, 2022.

[2] A. H. Siddique, S. Tasnim, F. Shahriyar, M. Hasan, and K. Rashid, "Renewable energy sector in Bangladesh: the current scenario, challenges and the role of IoT in building

https://doi.org/10.1155/2023/9998972 Published online by Cambridge University Press

a smart distribution grid," *Energies*, vol. 14, no. 16, p. 5083, 2021.

[3] G. Fan, Z. Liu, X. Liu et al., "Energy management strategies and multi-objective optimization of a near-zero energy community energy supply system combined with hybrid energy storage," *Sustainable Cities and Society*, vol. 83, Article ID 103970, 2022.

[4] S. Guo, K. Zheng, Y. He, and A. Kurban, "The artificial intelligence-assisted short-term optimal scheduling of a cascade hydro-photovoltaic complementary system with hybrid time steps," *Renewable Energy*, vol. 202, pp. 1169–1189, 2023.

[5] M. Ranjan and R. Shankar, "A literature survey on load frequency control considering renewable energy integration in power system: recent trends and future prospects," *Journal of Energy Storage*, vol. 45, Article ID 103717, 2022.

[6] A. G. Olabi, C. Onumaegbu, T. Wilberforce, M. Ramadan, M. A. Abdelkareem, and A. H. Al–Alami, "Critical review of energy storage systems," *Energy*, vol. 214, Article ID 118987, 2021.

[7] D. Xu, B. Zhou, N. Liu et al., "Peer-to-peer multienergy and communication resource trading for interconnected microgrids," *IEEE Transactions on Industrial Informatics*, vol. 17, no. 4, pp. 2522–2533, 2021.

[8] D. Groppi, A. Pfeifer, D. A. Garcia, G. Krajačić, and N. Duić, "A review on energy storage and demand side management solutions in smart energy islands," *Renewable and Sustainable Energy Reviews*, vol. 135, Article ID 110183, 2021.

[9] W. Guo and W. Xu, "Research on optimization strategy of harmonic suppression and reactive power compensation of photovoltaic multifunctional grid connected inverter," *International Journal of Electrical Power and Energy Systems*, vol. 145, Article ID 108649, 2023.

[10] L. Wang, H. Dong, J. Lin, and M. Zeng, "Multi-objective optimal scheduling model with IGDT method of integrated energy system considering ladder-type carbon trading mechanism," *International Journal of Electrical Power and Energy Systems*, vol. 143, Article ID 108386, 2022.

[11] L. Zeng, J. Xu, M. Wu et al., "Day-ahead interval optimization for CCHP system considering uncertainty of wind power and PV," *International Journal of Electrical Power and Energy Systems*, vol. 138, Article ID 107895, 2022.

[12] F. S. Gharehchopogh, "An improved Harris Hawks optimization algorithm with multi-strategy for community detection in social network," *Journal of Bionics Engineering*, vol. 20, no. 3, pp. 1175–1197, 2023.

[13] F. S. Gharehchopogh and T. Ibrikci, "An improved African vultures optimization algorithm using different fitness functions for multi-level thresholding image segmentation," *Multimedia Tools and Applications*, pp. 1–47, 2023, https://link.springer.com/article/10.1007/s11042-023-16300-1#article-info.

[14] F. S. Gharehchopogh and B. Abdollahzadeh, "An efficient Harris hawk optimization algorithm for solving the travelling salesman problem," *Cluster Computing*, vol. 25, no. 3, pp. 1981–2005, 2022.

[15] H. Mohammadzadeh and F. S. Gharehchopogh, "A multi-agent system based for solving high-dimensional optimization problems: a case study on email spam detection," *International Journal of Communication Systems*, vol. 34, no. 3, 2021.

[16] S. T. Shishavan and F. S. Gharehchopogh, "An improved cuckoo search optimization algorithm with genetic algorithm for community detection in complex networks," *Multimedia Tools and Applications*, vol. 81, no. 18, pp. 25205–25231, 2022.

[17] F. S. Gharehchopogh and A. A. Khargoush, "A chaotic-based interactive autodidactic School algorithm for data clustering problems and its application on COVID-19 disease detection," *Symmetry*, vol. 15, no. 4, p. 894, 2023.

[18] A. Walker and S. Kwon, "Design of structured control policy for shared energy storage in residential community: a stochastic optimization approach," *Applied Energy*, vol. 298, Article ID 117182, 2021.

[19] J. Nasiri and F. M. Khiyabani, "A whale optimization algorithm (WOA) approach for clustering," *Cogent Mathematics and Statistics*, vol. 5, no. 1, Article ID 1483565, 2018.

[20] W. Liu, Z. Guo, F. Jiang, G. Liu, D. Wang, and Z. Ni, "Improved WOA and its application in feature selection," *PLoS One*, vol. 17, no. 5, 2022.

[21] H. Liu, Y. Wang, S. Nie, Y. Wang, and Y. Chen, "Multistage economic scheduling model of micro-energy grids considering flexible capacity allocation," *Sustainability*, vol. 14, no. 15, p. 9013, 2022.

[22] J. Zhang, L. Hou, B. Zhang et al., "Optimal operation of energy storage system in photovoltaic-storage charging station based on intelligent reinforcement learning," *Energy and Buildings*, vol. 299, Article ID 113570, 2023.

[23] H. Feng, L. Zheng, and S. Qiao, "General layout planning model of landscape ceramic sculpture based on NSGA-II algorithm," *Scalable Computing: Practice and Experience*, vol. 24, no. 3, pp. 371–378, 2023.

[24] Y. Guan, M. Lv, S. Li, Y. Su, and S. Dong, "Optimized sensor placement of water supply network based on multi-objective white whale optimization algorithm," *Water*, vol. 15, no. 15, p. 2677, 2023.

[25] W. Yin and X. Qin, "Cooperative optimization strategy for large-scale electric vehicle charging and discharging," *Energy*, vol. 258, Article ID 124969, 2022.

[26] F. S. Gharehchopogh, M. H. Nadimi-Shahraki, S. Barshandeh, B. Abdollahzadeh, and H. Zamani, "Cqffa: a chaotic quasi-oppositional farmland fertility algorithm for solving engineering optimization problems," *Journal of Bionics Engineering*, vol. 20, no. 1, pp. 158–183, 2023.

[27] J. Zhang, M. Khayatnezhad, and N. Ghadimi, "Optimal model evaluation of the proton-exchange membrane fuel cells based on deep learning and modified African Vulture Optimization Algorithm," *Energy Sources, Part A: Recovery, Utilization, and Environmental Effects*, vol. 44, no. 1, pp. 287–305, 2022.

[28] Z. Gao, Y. Zhuang, C. Chen, and Q. Wang, "Hybrid modified marine predators algorithm with teaching-learning-based optimization for global optimization and abrupt motion tracking," *Multimedia Tools and Applications*, vol. 82, no. 13, pp. 19793–19828, 2023.

[29] V. Gerasimenko and I. Gapyak, "Propagation of correlations in a hard-sphere system," *Journal of Statistical Physics*, vol. 189, no. 1, p. 2, 2022.

[30] H. J. van Waarde, M. K. Camlibel, J. Eising, and H. L. Trentelman, "Quadratic matrix inequalities with applications to data-based control," *SIAM Journal on Control and Optimization*, vol. 61, no. 4, pp. 2251–2281, 2023.

[31] M. Balasubbareddy, D. Dwivedi, G. V. K. Murthy, and K. S. Kumar, "Optimal power flow solution with current injection model of generalized interline power flow controller using ameliorated ant lion optimization," *International Journal of Electrical and Computer Engineering*, vol. 13, no. 1, p. 1060, 2023.

https://doi.org/10.1155/2023/9998972 Published online by Cambridge University Press